Volume 1 | Number 1 | Jan 2013 | Pages 1–100

Dalton Transactions

An international journal of inorganic chemistry
www.rsc.org/dalton

ROYAL SOCIETY OF CHEMISTRY

This is an *Accepted Manuscript*, which has been through the Royal Society of Chemistry peer review process and has been accepted for publication.

Accepted Manuscripts are published online shortly after acceptance, before technical editing, formatting and proof reading. Using this free service, authors can make their results available to the community, in citable form, before we publish the edited article. We will replace this *Accepted Manuscript* with the edited and formatted *Advance Article* as soon as it is available.

You can find more information about *Accepted Manuscripts* in the **Information for Authors**.

Please note that technical editing may introduce minor changes to the text and/or graphics, which may alter content. The journal's standard **Terms & Conditions** and the **Ethical guidelines** still apply. In no event shall the Royal Society of Chemistry be held responsible for any errors or omissions in this *Accepted Manuscript* or any consequences arising from the use of any information it contains.

ROYAL SOCIETY OF CHEMISTRY

www.rsc.org/dalton

Dalton Transactions

ARTICLE TYPE

Ferrocene-appended ligands for use in spin crossover-redox "hybrid" complexes of iron(II) and cobalt(II)

Hayley S. Scott,[a] Christopher J. Gartshore ,[a] Si-Xuan Guo,[a] Boujemaa Moubaraki,[a] Alan M. Bond,[a] Stuart R. Batten,[a] and Keith S. Murray*[a]

In a study of multifunctional ('hybrid') molecular materials, with one function being spin-crossover and the second being reversible redox behaviour, we describe ferrocene-appended ligands and their d^6 and d^7 complexes *trans*-[$Fe^{II}(FTP)_2(NCS)_2$] (**1**), [$Co^{II}(FTP)_2$](ClO_4)$_2$·2(MeCN) (**2**) and
10 [$Fe^{II}(FTTP)_2$](ClO_4)$_2$·Et_2O (**3**) (where FTP = 4-(2-pyridyl)-1H-1,2,3-triazol-1-ylferrocene and FTTP = 4'-ferrocenyl-2,2':6',2''-terpyridine). The structures, magnetism and solution electrochemistry are described. Complex **1** remains high-spin, **2** displays gradual, incomplete spin crossover and **3** remains low-spin between 350 – 2 K. The electrochemical results show that one-electron oxidations at the ferrocene group, located external to the coordination site, occur at more positive potentials than the
15 'inner' $M^{II/III}$ couple in **1** and **2**, but not in **3**, and this has implications for retaining and influencing spin transitions at the M^{II} centres, in future..

Introduction

The use of multifunctional ligands in the field of spin crossover (SCO) is very topical with the secondary function, in the resulting
20 SCO metal complex, leading to associated properties such as porosity, electrical conductivity, magnetic order, liquid crystal, gels and non-linear optical activity.[1]

The current study was focused towards incorporating known ferrocenyl-based ligands, 4-(2-pyridyl)-1H-1,2,3-triazol-1-
25 ylferrocene, (labeled FTP)[2] and 4'-ferrocenyl-2,2':6',2''-terpyridine (labeled FTTP),[3] into Fe^{II} and Co^{II} mononuclear SCO complexes. Even though they are situated some distance from the SCO centre, this work aimed to investigate how one-electron changes at the ferrocene groups (*i.e.* Fe^{II}/Fe^{III}) would influence
30 the SCO behaviour at the $M^{II}(N)_6$ centres. This builds upon previous work where we reported a ferrocenyl-triazole based ligand and used it to form 1-D polymeric tris-1,2,4-triazole Fe^{II} complexes.[4]

The ferrocene containing ligands FTP and FTTP have previously
35 been synthesised and used in a variety of other work investigating their electrochemical,[2] optical[2] and biochemical[3] properties. Interestingly, this class of ligands has never been used for SCO purposes, despite non-ferrocene appended analogues appearing widely throughout the SCO literature.[5-9] Previously, non-
40 ferrocene appended analogues of FTP and FTTP have demonstrated the bidentate and *mer*-tridentate binding arrangement for these ligand types, respectively, to d-block ions.[6,10,11]

Reported here are the syntheses and properties of Fe^{II} and Co^{II}
45 mononuclear complexes formed from the FTP and FTTP ligands (Figure 1), of formulae [$Fe(FTP)_2(NCS)_2$] (**1**),

[$Co(FTTP)_2$](ClO_4)$_2$·2MeCN (**2**), and [$Fe(FTTP)_2$](ClO_4)$_2$·Et_2O (**3**).

Variable temperature magnetic susceptibility measurements and
50 single crystal structural analysis on compounds **1-3** have been performed.

To probe the redox features both at the ferrocene centres and at the central M^{II} 'core', particularly the order of potentials, electrochemical measurements were made on the FTTP free
55 ligand in acetonitrile solution and on the complexes **1 - 3** in DMF or MeCN, as appropriate.

60
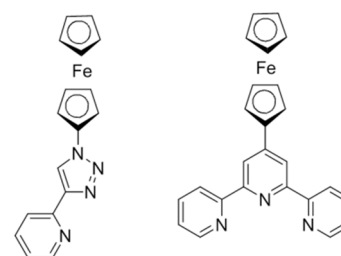
Figure 1. Molecular structure of ferrocene-appended ligands FTP (left) and FTTP (right).

Results and Discussion

Syntheses and Characterisation

70 For complex **1**, $Fe(ClO_4)_2$·$6H_2O$, NaNCS and FTP were reacted in a 1:2:2 mole ratio in methanol. After stirring, the solution was

filtered to remove any undissolved reactants and then the filtrate was left to sit in a sealed vial. Crystals of **1** were deposited after two days. To synthesise complexes **2** and **3**, FTTP and $M^{II}(ClO_4)_2 \cdot xH_2O$ (M = Co and Fe, as applicable) were dissolved
5 in MeOH in a 2:1 mole ratio. The solution was stirred, with heating, to precipitate a dark purple powder. The powder was filtered off and re-dissolved in MeCN, after which the solution was diffused with Et_2O to yield large purple block-shaped crystals of **2** and **3**. X-ray diffraction of these crystals using a
10 laboratory source diffractometer was not possible due to their very weakly diffracting nature, and so X-ray data for all structures reported (*vide infra*) were collected at the Australian Synchrotron. C, H, N data show that some solvate is lost upon exposure of crystals of **2** and **3** to air over extended periods.
15

Structural Descriptions

Compound **1** crystallises in the triclinic space group *P*-1 with structural data collected at 100 K. The central Fe^{II}, which lies on a centre of inversion, is coordinated by two FTP ligands binding
20 via the chelating triazole (N3) and pyridyl (N2) groups around the equatorial plane. Completing the FeN$_6$ donor set are two anionic $\underline{N}CS^-$ ligands which bind apically through the nitrogen (Figure 2). The Fe-N$_{(NCS)}$ bond distances is 2.100(2) Å, while the Fe-N$_{(FTP)}$ bond distances are 2.214(2) and 2.191(2) Å, typical of HS Fe^{II}.
25 Compound **1** displays a distorted octahedral geometry due to the chelating nature of the ligand with cis-N-Fe-N angles ranging between 76.16(8)-103.84(8)°. Selected bond lengths and angles for **1-3** are given in Table S1 (ESI). There are no solvent molecules in the outer coordination sphere and the closest
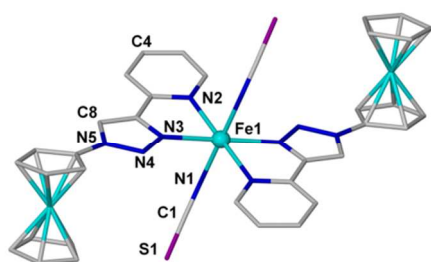30 intermolecular Fe…Fe distance is 7.940(1) Å.

35

Figure 2. Molecular structure of *trans*-[Fe(FTP)$_2$(NCS)$_2$] **1**. H atoms
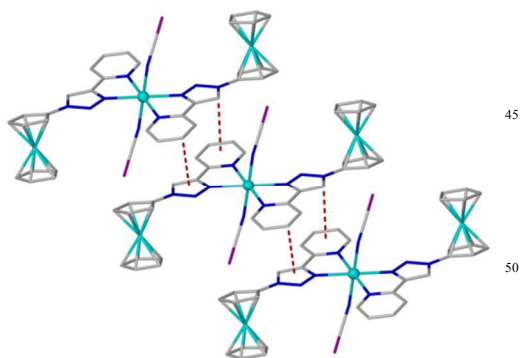40 omitted for clarity. Selected atoms are labelled.

45

50

55 **Figure 3.** π-π stacking between adjacent mononuclear complexes of **1**

60

There are off-set π-π stacking interactions between adjacent mononuclear complexes in **1** with centroid$_{pyridyl}$…C8 = 3.494 Å and centroid$_{triazole}$…C4 = 3.394 Å (Figure 3). There is also a H-
65 bonding interaction of (C8)H8...S1 = 2.684 Å between adjacent complexes. A list of closest contacts for complexes **1-3** appears in Table 1.

70 Compound **2** crystallises in the monoclinic space group $P2_1/n$ and its structure was collected at 100 K. The binding modes of the ligands to the metal centre are the same for complexes **2** and **3** and so only those for **2** will be described explicitly. Two terpyridine groups from the FTTP ligand chelate in a*mer* fashion
75 via the pyridylnitrogens. The three pyridyl rings for each ligand are coplanar, with the remaining three pyridyl groups on the other terpy moiety also coplanar but perpendicular to the first (Figure 4).

For **2**, at 100 K the two central pyridyl N-donors of each ligand
80 have an average Co-N$_{(FTTP)}$ distance of 1.897(5) Å and this is shorter than the average value of Co-N$_{(FTTP)}$ bond distances of the four 'side' pyridyl groups (2.077(5) Å). These Co–N distances are consistent with a Co^{II} occupying the LS state at this temperature. Compound **2** occupies a distorted octahedral
85 geometry with *cis* and *trans* N-Co-N angles ranging between 78.75(11)-106.12(11)° and 157.73(11)-174.88(11)°, respectively. There are two perchlorate anions in the outer coordination sphere, and two acetonitrile solvent molecules, one of which is disordered over two positions. There are a number of
90 intermolecular hydrogen bonds between the complex and the anion and solvent molecules (Table 1). The most significant is the π-π stacking that occurs between each ferrocene and a pyridyl group of an adjacent complex, resulting in an overall 1D-chain structure (Figure 5).
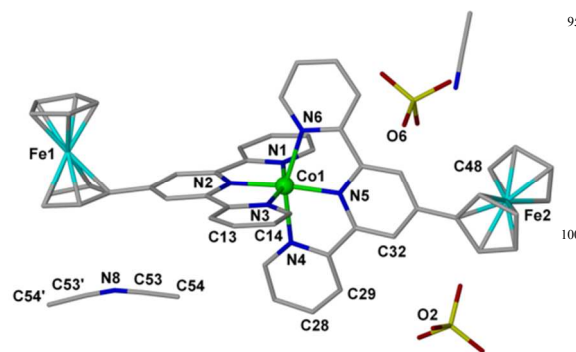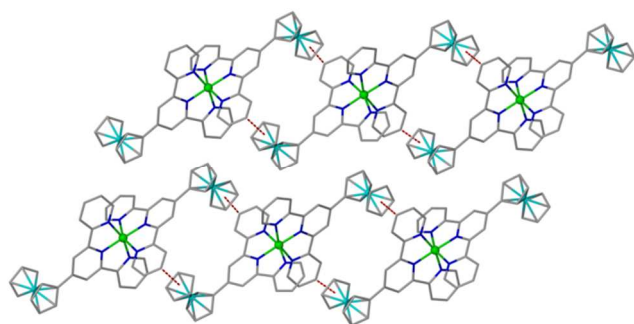
95

100

Figure 4. Structure and atom labeling in complex
105 [Co(FTTP)$_2$](ClO$_4$)$_2$·2(MeCN) **2**.

Figure 5. π-π stacking interactions (red lines) between the ferrocene and pyridyl moieties in **2**. Solvent, anions and H-atoms omitted for clarity.

5

Complex **3** crystallises in the monoclinic space group $P2_1/c$ and diffraction data were collected at 100 K (Figure 6). At this temperature the two central pyridyls of each ligand have an average Fe-N$_{(FTTP)}$ distance of 1.886(3) Å, this distance being

10 shorter than the average value of the Fe-N$_{(FTTP)}$ bond distances of the four side pyridyl groups (1.976(3) Å). These Fe-N distances are consistent with a Fe^{II} occupying the LS state. Compound **3** has a distorted octahedral geometry with *cis* and *trans* N-Fe-N angles ranging between 80.70(19)-101.7(2)° and 161.8(2)-177.20(19)°,

15 respectively. There are two perchlorate anions in the outer coordination sphere, and a single diethyl ether solvent molecule disordered over two positions (Figure 6).

There are a number of intermolecular hydrogen bonds occurring between the complex and the anion (Table 1). There is also a

20 CH…π interaction located between adjacent complexes resulting in an overall 1D supramolecular structure (Figure 7). This contrasts with the interactions found in substituted terpy analogues of type [Fe(R-terpy)$_2$]$^{2+}$ assemble into chains by virtue of π-stacking interactions between the R =

25 pyridylhydrazone units.[12]

30
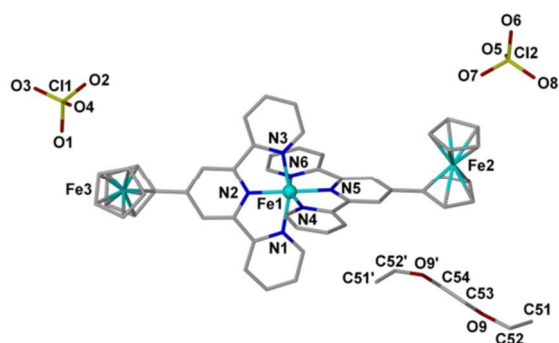
35 **Figure 6.** Structure and selected atom labeling in complex [Fe(FTTP)$_2$](ClO$_4$)$_2$·Et$_2$O **3**.

40
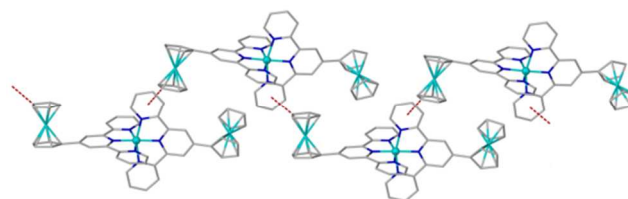
Figure 7. Supramolecular 1D chain structure of **3** showing CH…π interactions by a dotted red line. H-atoms and solvent molecules omitted for clarity.

45

Table 1. Intermolecular interactions present in complexes **1**, **2** and **3**

D-H···A	D-H (Å)	H···A(Å)	D···A(Å)	D-H···A °
1 C8-H8···S1^i	0.95	2.684	3.606(8)	173.5
Centroid(N3-C7)···C4^{ii}	-	-	3.394	-
Centroid(N2-C6)···C8^{ii}	-	-	3.494	-
2 C32-H32···O2	0.95	2.668	3.610(6)	171.7
C29-H29···O2	0.95	2.525	3.465(6)	170.3
C48-H48···O6	0.95	2.603	3.418(6)	124.6
Centroid(C46-C50)…C13^{iii}	-	-	3.324	-
Centroid(C21-C25)…C28^{iv}	-	-	3.357	-
3 C13-H13…O4^v	0.95	2.532	3.327(9)	141.3
C12-H12…O6^{vi}	0.95	2.532	3.478(8)	173.7
C28-H28…O6^{vii}	0.95	2.655	3.364(8)	131.8
C12-H12…O7^{vi}	0.95	2.550	3.257(8)	131.3
Centroid(N3-C15)…H48C48^{viii}	0.95	2.897	3.698	142.7

Symmetry operations: (i) x-1, y, z; (ii) 1-x, 1-y, -z; (iii) ½+x, ½-y, ½+z;
50 (iv) x-½, ½-y, z-½, (v) –x, 1-y, -z; (vi) –x, 2-y, -z; (vii) x, 5/2-y, ½+z;
(viii) –x, y-½, ½-z.

Magnetic Behaviour

Direct current (dc) magnetic susceptibility measurements were performed on polycrystalline complexes **1** - **3** under an applied
55 field of 0.5 T. Their $\chi_M T$ vs. *T* plots appear in Figure 8.

Complex **1** remains HS d^6 (^{5}T$_{2g}$ parent state) over the temperature range 2 - 300 K (Figure 8(a)). Beginning at 300 K, a $\chi_M T$ value of 3.98 cm^3 mol^{-1} K (μ_{eff} = 5.65 μ_B) remains essentially constant following cooling down to 50 K, below which point further
60 cooling to 2 K yields a more rapid reduction to 2.50 cm^3 mol^{-1} K due to spin-orbit/low symmetry splittings leading to zero field splitting effects on the resultant ^{5}A$_{2g}$ state.

Complex **2** shows an initial $\chi_M T$ value of 1.35 cm^3 mol^{-1} K (μ_{eff} = 3.29 μ_B) at 340 K then a reduction in $\chi_M T$ occurs as the sample is
65 cooled to 150 K where a $\chi_M T$ value of 0.42 cm^3 mol^{-1} K is observed (Figure 8(b)). Further cooling beyond this point leads to plateau values in $\chi_M T$, reaching 0.38 cm^3 mol^{-1} K (μ_{eff} = 1.74 μ_B) at 5 K. The plot is typical of a gradual, incomplete $S = ½ \leftrightarrow S = 3/2$ crossover.[8,9]

70 Variable temperature magnetic susceptibility data for compound **3** revealed, through its diamagnetism, that it occupies the LS state between 2 - 350 K (Figure 8(c)). This formation of the LS state in Fe^{II}, compared to SCO for the Co^{II} analogue, is common for [Fe(terpy)$_2$]$^{2+}$ type species.
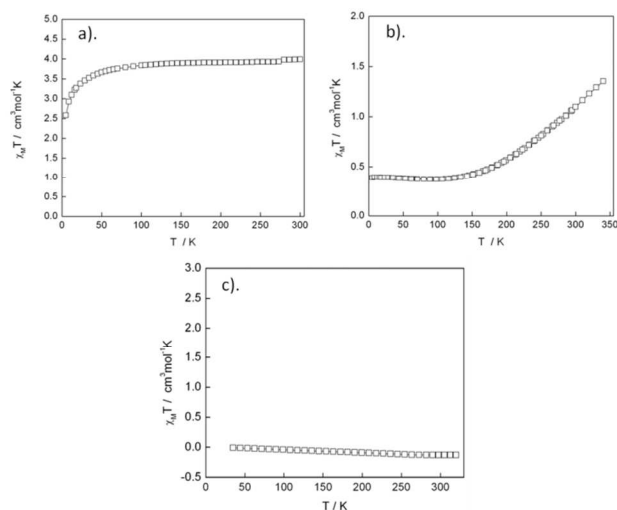
75

Figure 8. $\chi_M T$ vs. T plots for complexes **1** (a), **2** (b) and **3** (c).

Electrochemical Studies

The electrochemistry of the free ligands, FTP and FTTP, as well as complexes **1** - **3** was investigated under transient conditions using cyclic voltammetry (CV) at macrodisk electrodes and near steady-state ones using voltammetry at microdisk electrodes at 22 ± 2 ºC in DMF or MeCN (as relevant) containing 0.05 M of [Bu$_4$N][ClO$_4$] as the supporting electrolyte. A summary of potentials derived for complexes **1** - **3** and both ligands appears in Table 2.

Cyclic voltammograms of a 0.5 mM solution of **1** in DMF shows a one-electron chemically reversible process labelled **II** in Figure 9 with a peak-to-peak separation ($\Delta E_p = E_p^{ox} - E_p^{red}$ where superscripts *ox* and *red* designate the oxidation and reduction components respectively) of about 70 mV at a scan rate of 100 mV s^{-1}. When the potential is immediately switched after process **II**, a ΔE_p value of 90 mV is obtained at a scan rate of 100 mV s^{-1}, and the ratio of I_p^{ox}/I_p^{red} is close to unity, and subtle differences emerge with the different switching potentials employed. The formal reversible potential ($E^{0'}_f(n) = (E_p^{ox} + E_p^{red})/2$) is -150 mV versus [Fc]$^{0/+}$ for process **II**, which is attributed to the one-electron oxidation of Fe(II) to Fe(III). The peak current is proportional to the square root of the scan rates in the range of 0.05 V s^{-1} to 1 V s^{-1}, indicating this process is diffusion controlled at the peak potential. The diffusion coefficient calculated using the Randles-Sevcik[13] relationship is 4.4 (± 0.2) × 10^{-6} cm s^{-1}. There is also a large partially chemically reversible oxidation process (**I**) with an approximate $E^{0'}_f$ value of 210 mV (Figure 9a) and a ΔE_p value of 105 mV whose characteristics change with each cycle of potential, and an irreversible oxidation process (**III**) with a peak potential of 710 mV (not shown).

The FTP ligand shows a close to reversible oxidation process (Figure S1) with an $E^{0'}_f$ value of 205 mV when the potential is switched soon after the peak potential. This process is assigned to the oxidation of the Fc moiety of the ligand to the corresponding ferrocenium cation. A second oxidation process with a peak potential of 655 mV is observed when the potential is scanned to more positive values, which is associated with the pyridyl-triazole ligand. On the basis of these data, process **I** for complex **1** is assigned to oxidation of the Fc moiety of FTP,

while **III** is due to the oxidation of the pyridyl-triazole ligand. Under steady state conditions at a carbon fibre microelectrode, only the Fc oxidation component is well defined, showing that the electrode kinetics of the ligand oxidation process detected at a more positive potential is complicated.

If the voltammetry of **1** were totally straightforward and consisted of two simple diffusion controlled reversible one electron oxidation processes then their peak height ratio should be close to unity. However, on the first cycle of potential the peak current for process **I** is about four times that of **II**, although there are only two Fc centres to be oxidised in complex **1**. One plausible explanation is that the $\pi - \pi$ stacking is strong with the initial species and its diffusion coefficient is lower than for a monomer. This can give rise to complexities in the voltammetry.[14] Plausibly, after Fe(II) is oxidized to Fe(III), the $\pi - \pi$ stacking is broken so the oxidised species has significantly higher diffusion coefficient than **1**, giving rise to complexities in the mass transport. This hypothesis is supported by the fact that when the potential is switched after process **I**, on the second and subsequent cycles, the peak current of process **II** increases, and as expected is now about half of that for process **I**. Under some circumstances, this monomer-oligomer transition could display concentration dependent effects. However, voltammetric studies carried out at a lower concentration of 0.10 mM for **1** show similar characteristics to those at 1.0 mM. NMR spectra obtained at concentrations of 0.01 mM to 10 mM also have the same chemical shifts.

Anomalies in mass transport also emerge in studies with microelectrodes. The near steady-state microelectrode data for **1** showed a limiting current ratio of about 4 to 1 times for processes **II** and **I** (Figure 9b), akin to the peak current ratio found in cyclic voltammetry. The diffusion coefficient (*D*) is calculated from the near steady state current (I_{ss}) for process **II** using the microelectrode equation[15] $I_{ss} = 4nFDCr$ where *n* is the number of electron transferred, *C* is the bulk concentration, *r* is the radius of the microelectrode and F is Faraday's constant. The diffusion coefficient calculated from the near steady state voltammogram for process **II** gives a value of 4.3 × 10^{-6} cm s^{-1}, which is consistent with the results obtained from the cyclic voltammograms. The steady state voltammogram at 0.1 mM shows the same current ratios for the two oxidation processes. The basic scheme proposed that process **II** is derived from oxidation of Fe(II) and process **I** from oxidation of the two ferrocene centres is clear, but subtleties in mass transport properties are evident and of unknown origin.
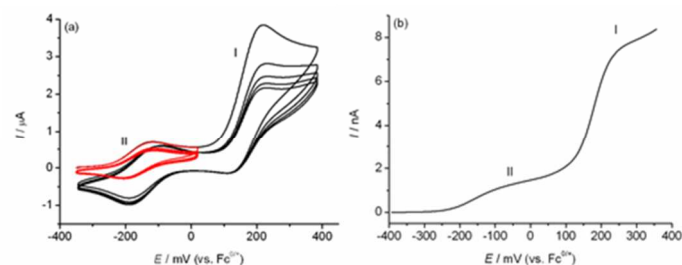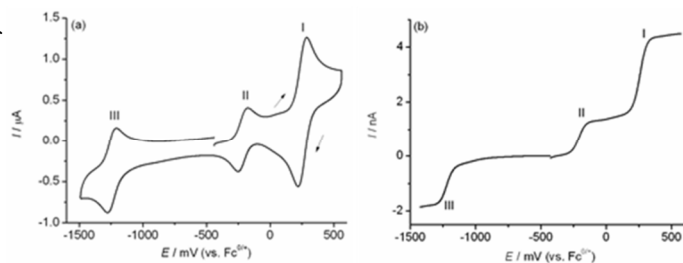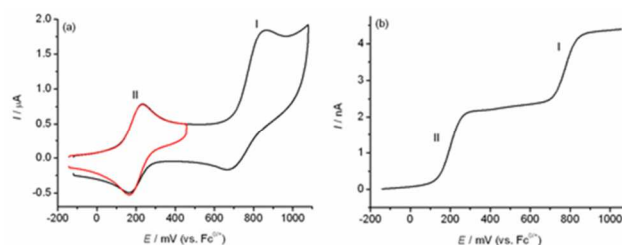

Figure 9. Cyclic (a) and near steady-state (b) voltammograms of 0.5 mM **1** in DMF (0.05 M [Bu$_4$N][ClO$_4$]), obtained with a 1 mm dia. glassy carbon disk electrode at a scan rate of 100 mV s^{-1}, and a 36.5 µm dia. carbon fibre electrode at a scan rate of 5 mV s^{-1}, respectively.

Cyclic voltammetric studies of a 0.5 mM solution of $[Co^{II}(FTTP)_2](ClO_4)_2 \cdot 2(MeCN)$ **2** in acetonitrile (0.05 M $[Bu_4N][ClO_4]$), exhibit three well-separated processes labelled **I**, **II** and **III** in Figure 10a. Their formal potentials ($E^{0'}_f$ (n), n = **III**,
5 **II**, **I**) are -1238, -214, and 269 mV, respectively. All three processes are both chemically and electrochemically reversible as evidenced by the near unity of the I_p^{ox}/I_p^{red} ratio at all scan rates studied and the ΔE_p values of about 70 mV for each process at a scan rate of 100 mV s^{-1}, but while the current magnitude for
10 processes **II** and **III** are similar, that for process **I** is about twice their magnitude. The oxidation peak current (I_p^{ox}) of process **II** was used for the calculation of the diffusion coefficient of complex **2**. The plot of I_p^{ox} value versus the square root of the scan rate for the range of 0.05 V s^{-1} to 1 V s^{-1} was linear and
15 passed through the origin, indicating that this process is diffusion controlled. A diffusion coefficient of 2.2 (± 0.2) × 10^{-6} cm s^{-1} was calculated using the Randles-Sevcik equation. There are also a large irreversible oxidation process at 1298 mV and a large irreversible reduction process at -1498 mV, which are attributed
20 to the oxidation and reduction of the FTTP ligand, respectively. The free ligand FTTP shows two processes having significant chemical reversibility with $E^{0'}_f$ values of 115 mV and 740 mV (see ESI, Figure S2), and one irreversible oxidation and one irreversible reduction processes close to the solvent limit. The
25 process at 115 mV is attributed to oxidation of the Fc moiety from the FTTP ligand. However, the near steady-state voltammogram obtained at a 36.5 μm dia. carbon fibre electrode as was the case with oxidation of FTP at this electrode, discriminates heavily against the second process indicating
30 significant kinetic control on the short time scale of the microelectrode voltammetry of the ligand.

The near steady-state voltammogram of complex **2** obtained at a 36.5 μm dia. carbon fiber electrode (Figure 10b) revealed processes **I** and **II** with $E_{1/2}$ values of 263 and -214 mV,
35 respectively. Both processes exhibit positive, that is, oxidation, currents. Process **I** has a steady state current which is about twice that of process **II**, and is assigned to a two-electron oxidation of the Fc moieties from the FTTP ligands, while process **II** is assigned to a one-electron oxidation of Co(II) to Co(III). Process
40 **III**, ($E_{1/2}$(**III**) = -1075 mV), exhibits a negative or reduction current, and hence is assigned to a reversible one-electron reduction processes of Co(II) to Co(I). However, the diffusion coefficient calculated from the steady state limiting current of process **II** and the I_{ss} eqn.[15] gives a value of 4.5 (± 0.2) × 10^{-6} cm
45 s^{-1}, which is about twice that obtained by cyclic voltammetry. The limiting current value from a near steady state voltammogram obtained from a 7 μm diameter carbon fiber electrode also gave a similar value. Cyclic and near steady state voltammetric data obtained at the lower concentration of 0.25 mM also displayed
50 the same discrepancy in diffusion coefficient evaluation. The reason for this discrepancy in the mass transport parameter, like the one noted for **I** above with relative current magnitudes is yet to be resolved, but agreement with respect to potential and other thermodynamic aspects again is achieved. Since the anomalous
55 mass transport features give rise to technique dependent diffusion coefficients, they should be regarded as D_{app} or apparent diffusion coefficient values.

Figure 10. Cyclic (a) and near steady-state (b) voltammograms of 0.42
60 mM **2** in MeCN (0.05 M $[Bu_4N][ClO_4]$), obtained with a 1 mm dia. glassy carbon disk electrode at a scan rate of 100 mV s^{-1} and a 36.5 μm dia. carbon fibre electrode at a scan rate of 5 mV s^{-1}, respectively.

Figure 11. Cyclic (a) and near steady-state (b) voltammograms of 0.5
65 mM **3** in MeCN (0.05 M $[Bu_4N][ClO_4]$), obtained with a 1 mm diameter glassy carbon disk electrode at a scan rate of 100 mV s^{-1} and a 36.5 μm diameter carbon fibre electrode at a scan rate of 5 mV s^{-1}, respectively.

Table 2. Summary of redox processes detected for complexes **1-3** using
70 cyclic voltammetry and comparisons to $[Co(terpy)_2]^{2+}$ and $[Fe(terpy)_2]^{2+}$.[a] Irreversible process; [b]$vs.$ Fc$^{0/+}$; [c] ferrocene group; [d] (converted from Ag/AgCl; satd.NaCl in MeCN)[16];[e] converted from SSCE in MeCN.[17]

Complex/ Compound	Process		$E_{1/2}$ (mV)[b]	$E_{1/2}$ (mV) $[M(terpy)_2]$ examples
1	FTP/FTP^{+c}	**I**	210	-
	Fe^{II}/Fe^{IIIa}	**II**	-155	-
FTP	FTP^{+}/FTP^{2+}		700[d]	
	FTP^{+}/FTP^{+}		205	
2	FTTP/FTTP^{+c}	**I**	270	-
	Co^{II}/Co^{III}	**II**	-215	-140[d]
	Co^{II}/Co^{I}	**III**	-1240	-1180[d]
3	Fe^{II}/Fe^{III}	**I**	765	680[d], 710[e]
	FTTP/FTTP^{+c}	**II**	200	-
FTTP	FTTP^{+}/FTTP^{2+}		740	
	FTTP/FTTP^{+}		115	

Cyclic voltammograms of a 0.5 mM solution of **3** in
75 acetonitrile (0.05 M $[Bu_4N][ClO_4]$) exhibit two well-separated, one-electron, processes labelled **I** and **II** in Figure 11a. Their formal potentials ($E^{0'}_f$ (n), n = **II** to **I**) are about 200 and 770 mV, respectively. The ΔE_p value of 70 mV at a scan rate of 100 mV s^{-1}, and the fact that the I_p^{ox}/I_p^{red} ratio is almost unity at all scan
80 rates when the potential is switched prior to the onset of process **I** shows that process **II** is chemically and electrochemically reversible. The ΔE_p value of 200 mV for process **I** at a scan rate of 100 mV s^{-1} and the non-unity peak current ratio indicates that this is not a fully reversible process, although the close proximity
85 to further oxidation at 1000 mV introduces some uncertainty into this value and to the peak current ratio. Both processes occur at

slightly more positive potentials than found for the free ligand FTTP. There is also a large, chemically irreversible reduction process at -2055 mV (not shown) which is attributed to the reduction of the FTTP ligand, as observed in the cyclic voltammograms of the free ligand and complex **2**. The diffusion controlled nature of process **II** is confirmed by the linear relationship between the I_p values and the square root of the scan rate over the range of 0.05 V s^{-1} to 1 V s^{-1}, which also passes through the origin. The apparent diffusion coefficient calculated using these data for process **II** and the Randles-Sevcik equation is 3.3 ($\pm$0.2) $\times$ 10^{-6} cm s^{-1}.

The near steady-state voltammogram of **3** obtained at a 36.5 μm carbon fibre electrode (Figure 11b) reveals that processes **I** and **II** ($E_{1/2}$ (**I**) = 765 and 200 mV) exhibit positive oxidative limiting currents with similar magnitude. Unlike the ligand, complex **3** shows two well defined one-electron oxidation steps in the near steady-state voltammogram having similar limiting current values. Thus, by comparison with the Co-analogue, processes **I** and **II** are tentatively assigned to the one-electron oxidation of Fe(II) to Fe(III) and FTTP to FTTP$^+$, respectively. However, similar to the Co-analogue, the apparent diffusion coefficient of 6.0 $\times$ 10^{-6} cm s^{-1} calculated from the near steady state current of process **II** and the I_{ss} equation[15] is again about twice the value obtained from cyclic voltammetry.

Discussion

Magnetism

Non-ferrocene appended analogues to FTP (*i.e.* substituted 1,2,3-triazole-4-(2-pyridyl) ligands; Fig. 1), have previously been used to chelate to metal ions via the triazole N(3) and the pyridyl N donors.[18] Close azole relatives to FTP such as pypzH = 2-(1H-pyrazol-3-yl)-pyridine and tzpy = 3-(2-pyridyl)[1,2,3]triazolo[1,5-a]pyridine, have also been incorporated into Fe(II) SCO complexes similar in nature to **1**. For example, ligand-NH hydrogen-bonded bridges gave pseudo-dimeric complexes {*cis*-[Fe(pypzH)$_2$(NCX)$_2$]$_2$-(μ-OH$_2$)(H$_2$O)$_2$}·H$_2$O·MeOH (where X = S or Se). The NCS complex remained HS at all temperatures, while the NCSe complex showed SCO in the solvated form.[5]

Additionally, a study by Sheu *et al.*,[6] reported two polymorphs of *trans*-[Fe(tzpy)$_2$(NCS)$_2$] and found that both displayed abrupt SCO. Polymorph A showed a $T_{1/2}$ ~ 150 K while polymorph B showed $T_{1/2}$ ~102 K. Apart from different ligand field strengths for tzpy compared to FTP, the occurrence of SCO for these compounds could be due to the molecules in the crystal forming a sheet structure along the *ac* and *ab* plane for A and B, respectively, and yielding π–π interactions between adjacent parallel tzpy planes. Earlier work by Gaspar *et al.*, also using the ligand tzpy, has yielded similar SCO complexes.[11]

From the measurements reported on triazole-pyridine-based [Fe(L)$_2$(NCS)$_2$] complexes, either *cis* or *trans* disposed, it is clear that the magnetic behaviour is highly dependent on factors such as the nature of the counter-anions, solvent and intermolecular interactions operating between monomers, since all compounds have similar coordination sphere. The present ferrocene-functionalised example **1** remained HS at all temperatures, despite similar compounds displaying spin transitions. Estimation of the ligand field provided by FTP will require measurement of

the visible spectrum of a Ni(II) analogue.[4]

The magnetic and electrochemical properties of non-Fc analogues of **2** and **3** {[Co^{II}(terpy)$_2$]$^{2+}$ and [Fe^{II}(terpy)$_2$]$^{2+}$} are well known.[8,9,12,16,17] All known salts of [Fe^{II}(terpy)$_2$]$^{2+}$ remain LS at all temperatures. This has previously been accounted for as being due to the strong π-acceptor and σ-donor metal–ligand interactions generating a large ligand field splitting between the metal-localised dπ and dσ* molecular orbitals.[7] Here we have found that attaching a ferrocene group to the 4-position of the central pyridine does not affect the ligand field contribution enough to induce a thermally accessible spin transition in Fe(II) complexes such as in **3**, that remains low spin.

In the case of the Co^{II} complex **2**, SCO does occur and is typical of a gradual, partial d^7 spin transition that does not fully occupy the HS S = 3/2 state at 340 K. The LS plateau for S = 1/2 has a $\chi_M T$ value typical of [Co(terpy)$_2$]$^{2+}$ cations, as does the gradual spin transition, with $T_{1/2}$ ~350 K. For example [Co(terpy)$_2$](ClO$_4$)$_2$·1.5H$_2$O shows μ_{eff} = 4.18 μ_B at 342 K indicative of more HS population (*i.e.* weaker ligand field) compared to **2** at this temperature.[19] It is to be noted that Hayami *et al.*,[8] and others,[9] have done a large amount of work synthesising alkyl chain-, aromatic chain- and other R-substituted terpy derivatives for use in Co(II) SCO complexes and, in distinction to Fe^{II}, many of these exhibit gradual SCO while others show 'reverse SCO' *i.e.* low spin to high spin on decreasing temperature. Complex **2** falls into the normal, gradual transition category In addition, Constable *et al.*[12] have made extensive studies of Fe(II) (and Ru(II)) substituted-terpy complexes, incorporating pyridine groups onto the 4-position of the central terpy-pyridyl group. This work showed the formation of extended networks, exhibiting π-π stacking between pendant rings, the complexes remaining low spin.

Electrochemistry

We have presented a detailed study of the electrochemical properties of complexes **1** to **3** with the assigned redox couples given in Table 2. While the reported potentials and other thermodynamic parameters are as expected and technique independent, there are unusual and, as yet, unexplained anomalies in the mass transport that are reflected in differences in relative current magnitudes and apparent diffusion coefficient values derived from cyclic voltammetric peak current magnitudes under transient conditions at macrodisk electrodes and near steady state limiting currents found at slow scan rates with microelectrodes. It remains to be seen if this and other mass transport anomalies are seen in future studies with other ferrocene-substituted metal complexes.

In regard to the potentials and redox processes, comments are now given on 'parent' terpy complexes [Co^{II}(terpy)$_2$](ClO$_4$)$_2$ and [Fe^{II}(terpy)$_2$](ClO$_4$)$_2$. Using cyclic voltammetry, Rao *et al.*,[16] found that [Co^{II}(terpy)$_2$]$^{2+}$ underwent a one electron oxidation step, [Co^{II}(terpy)$_2$]$^{2+}$ to [Co^{III}(terpy)$_2$]$^{3+}$, and three one-electron reductions: [Co^{II}(terpy)$_2$]$^{2+}$ to [Co(terpy)$_2$]$^{1+}$; [Co(terpy)$_2$]$^{1+}$ to [Co(terpy)$_2$]^0; and [Co(terpy)$_2$]^0 to [Co(terpy)$_2$]$^{1-}$. They employed formal oxidation state nomenclature +2, +1, 0 and -1 and noted that redox processes could be associated with the metal or at the terpy ligand orbitals. Later Morris *et al.* used ESR to monitor the spin of the reduced states, all showing S = ½ and indicative of

reductions occurring at the ligand centres.[17] Comparing the present FTTP work to the abovementioned terpy complexes, only the reductive process, $[Co(FTTP)_2]^{2+}$ to $[Co(FTTP)_2]^{1+}$ was observed for **2** (Table 2).

In the case of $([Fe^{II}(terpy)_2]^{2+}$, reductions to form $[Fe(terpy)_2]^{1+}$ and then $[Fe(terpy)_2]^{1+}$ to $[Fe(terpy)_2]^{0})[16]$ were possible but these could not be seen in the FTTP system, **3**. Complexes **2** and **3** both showed one-electron oxidations to the Co[III] and Fe[III] formal oxidation states. Importantly, oxidation of the appended ferrocene group to the ferrocenium state is observed at potentials a little more positive than that of free ferrocene but we have thus far not been able to isolate the ferrocenium complexes of the M(II) complexes by controlled potential electrolysis. This relates, at least in **2**, to the FTTP/FTTP$^+$ potential being more positive than the M[III/II] potential thus leading to M[III] formation. Further work is required.

In summary, the new complexes **1** to **3** have been successfully synthesised and structurally characterised, together with detailed probing of their solution electrochemistry. The initial aim of elucidating the effect that redox function, at the peripheral ferrocene moiety, *viz*. Fc to Fc$^+$, might have, or not have, upon spin crossover features at the central Fe[II] or Co[II] ion has not been possible, to date, probably for the relative redox potential reason given above. In general, the Fc-substituted ligands, FTP and FTTP, do not produce any dramatic spin crossover effects though FTTP modulates the spin states somewhat compared to terpy in analogous Co[II] and Fe[II] species.

Experimental

General

Elemental analyses (C, H, N) were performed by the Campbell Microanalytical Laboratory, University of Otago, Dunedin, New Zealand. Infrared spectra were recorded on a Bruker Opus/IR IFS 55 spectrophotometer in the range 4000–400 cm^{-1}.Ligands FTP and FTTP were made using previously reported methods.[2,3]

Variable temperature magnetic susceptibility data were collected using either a Quantum Design MPMS 5 Superconducting Quantum Interference Device (SQUID) magnetometer or a MPMS XL-7 SQUID magnetometer, with a scan speed of 10 K / min followed by a one minute wait after each temperature change.

Cyclic voltammograms were acquired at 22 ± 2 °C using a BAS 100B (Bioanalytical Systems, Inc.) or a CHI 760E electrochemical workstation (CH Instruments, Austin, Texas, USA). A standard three-electrode electrochemical cell arrangement was employed using glassy carbon (1.0 mm diameter, CH Instruments, Austin, Texas, USA), or a 33 μm diameter carbon fibre (ALS Co., Japan) working electrode, a Pt wire counter electrode and a Pt wire in a tip separated from the bulk solution which was used as the quasi-reference electrode. All potentials were referred to the reversible potential for the ferrocene/ferrocenium ion (Fc/Fc$^+$) couple using measurements derived from the oxidation of Fc as an external reference. The effective areas of the macrodisk GC electrodes were determined by measurement of the reduction of 1.0 mM K$_3$[Fe(CN)$_6$] in water (0.5 M KCl) by cyclic voltammetry and use of the Randles-Sevcik equation with a known diffusion coefficient of 7.6×10^{-6}

cm^2 s^{-1} for [Fe(CN)$_6$]$^{3-}$. The actual diameter of the carbon fibre electrode (36.5 μm) was also measured in 1.0 mM K$_3$[Fe(CN)$_6$] solution by near steady state voltammetry and the use of the microelectrode I_{SS} equation.[15] The working electrodes in all experiments were polished, cleaned, rinsed with water and then acetone, and dried under nitrogen before use. The solution was purged with nitrogen for at least 10 min before measurement for complete removal of O$_2$, and then the electrochemical cell was kept under a positive pressure of nitrogen at all times. 0.05 M of

Compound	1	2	3
Formula	C$_{36}$H$_{28}$N$_{10}$Fe$_3$S$_2$	C$_{54}$H$_{41}$Cl$_2$CoFe$_2$N$_8$O$_8$	C$_{54}$H$_{38}$Cl$_2$Fe$_3$N$_6$O$_9$
Mw (g mol^{-1})	832.34	1117.48	115.35
T (K)	100(2)	100(2)	100(2)
Crystal system	Triclinic	Monoclinic	Monoclinic
Space group	*P*-1	*P*2$_1$/*n*	*P*2$_1$/*c*
Z	1	4	4
a (Å)	7.9400(16)	12.802(3)	12.883(3)
b (Å)	10.660(2)	18.888(4)	21.216(4)
c (Å)	11.810(2)	20.634(4)	19.747(4)
α (°)	113.84(3)	90	90
β (°)	92.39(3)	96.30(3)	106.19(3)
γ (°)	108.15(3)	90	90
V (Å^3)	852.5(3)	4959.2(17)	5091.7(18)
ρ_{calc} (g cm^{-3})	1.621	1.569	1.505
μ (mm^{-1})	1.427	1.082	1.012
Measured/independent (R$_{int}$) Reflections	27273/3764(0.0484)	106565/14615(0.0611)	96072/14467(0.0728)
Observed reflections [I > 2σ(I)]	3388	10895	10422
R$_1$^{a}, *w*R$_2$^{b}[I > 2σ(I)]	0.0391, 0.0982	0.0647, 0.1789	0.0966, 0.2568
R$_1$, *w*R$_2$ (all data)	0.0433, 0.1006	0.0870, 0.1936	0.1259, 0.2760
Goodness-of-fit on F^2	1.090	1.042	1.083

[Bu$_4$N][ClO$_4$] was used as the supporting electrolyte.

Table 3. Crystallographic details for complexes **1-3**.

^{a}R$_1$ = $\sum||F_o| - |F_c||/\sum|F_o|$. ^{b}*w*R$_2$ = $\{\sum[w(F_o^2\sum F_c^2)^2]/\sum[w(F_o^2)]\}^{1/2}$.

X-Ray crystallographic measurements were performed at 100(2) K for **1**, **2** and **3** at the Australian Synchrotron MX2 beam-line. The data collection and integration were performed within the Blu-Ice[20] and XDS[21] software programs. Crystallographic data and refinement parameters for **1-3**, given in Table 3, were solved by direct methods (SHELXS-97), and refined (SHELXL-97) by full least-squares on all F^2 data.[22] Unless stated otherwise, all non-hydrogen atoms in **1-3** were refined anisotropically and all hydrogen atoms were placed in calculated positions.

The crystal structure of **2** contains positional disorder in one of the acetonitrile solvent molecules; that is, carbon atoms C53 and C54 are disordered over two positions in a ratio of 1:1 with C53' and C54'. The entire solvent molecule was made isotropic and no hydrogen atoms were assigned. DFIX restraints were placed on the atom pairs C53/C54 and C53'/C54' with a distance of 1.45(1) Å; and N8/C53 and N8/C53', with a distance of 1.13(1) Å.

The crystal structure of **3** contains disorder in the diethyl ether solvent molecule; that is, atoms C51, C52 and O9, are disordered over two positions in a ratio of 1:1 (with C51', C52' and O9'). The entire solvent molecule was made isotropic and no hydrogen atoms were assigned. DFIX restraints were placed on the atom pairs C51/C52, C52/O9, O9/C59, C53/C54, C54/O9', O9'/C52' and C52'/C51' with a distance of 1.40(1) Å. DANG restraints were placed on the atom pairs C51/O9, O9/C54, C53/O9', C54/C52' and O9'/C51 with a distance of 2.38(1) Å.

Metal Complex Syntheses

[Fe^{II}(FTP)$_2$(NCS)$_2$] (1)

FTP (10 mg, 0.03 mmol), NaNCS (2.45 mg, 0.03 mmol) and Fe(ClO$_4$)$_2$.6H$_2$O (3.8 mg, 0.015 mmol) were dissolved in 5 ml MeOH with 5 mg ascorbic acid added to prevent Fe^{II} oxidation. The solution was stirred for 30 minutes, after which time a yellow solution had formed. The solution was filtered and the filtrate left to sit in a sealed vial. Crystals of diffraction quality formed after two days. Mw 832.34; Yield 8 mg (64 %); IR(cm^{-1}, room temperature) 3063 (s), 2037 (s), 1653 (s), 1605 (s), 1572 (s), 1512 (m), 1447 (s), 1410 (m), 1291 (s), 1256 (s), 1192 (m), 1157 (m), 1103 (m), 1078 (s), 1048 (m), 1030 (m), 875 (s), 819 (s), 777 (s), 742 (s), 704 (m), 635 (w); Anal. Found C 51.89, H 3.52, N 16.70; Calcd for C$_{36}$H$_{28}$N$_{10}$Fe$_3$S$_2$, C 51.95, H 3.39, N 16.83.

[Co^{II}(FTTP)$_2$](ClO$_4$)$_2$·2MeCN (2)

FTTP (20 mg, 0.048 mmol) and Co^{II}(ClO$_4$)$_2$·6H$_2$O (8.7 mg, 0.024 mmol) were dissolved in 5 ml MeOH and stirred with light heating for 30 minutes. After this time, the precipitate that formed was filtered and washed with a further 2 ml MeOH and then re-dissolved in a small amount of MeCN. The subsequent solution was placed in an open vessel within a vapour-diffusion chamber containing diethyl ether, giving purple crystals that were suitable for X-ray crystallographic analysis. Mw 1171.48; Yield 11 mg (41 %); IR (cm^{-1}, room temperature) 3105 (s), 3081 (s), 2294 (s), 1601 (s), 1567 (s), 1541 (s), 1496 (s), 1468 (s), 1432 (s), 1412 (s), 1251 (s), 1167 (s), 1070 (br), 883 (s), 844 (m), 788 (s), 768 (s), 749 (s), 731 (s), 672 (s), 655 (s), 619 (s); Anal. Found C 54.00, H 3.81, N 8.22; Calcd for C$_{50}$H$_{38}$N$_6$Fe$_2$Co$_1$Cl$_2$O$_8$, C 54.97, H 3.51, N 7.69.

[Fe^{II}(FTTP)$_2$](ClO$_4$)$_2$·Et$_2$O (3)

FTTP (20 mg, 0.048 mmol) and Fe^{II}(ClO$_4$)$_2$·6H$_2$O (8.7 mg, 0.024 mmol) were dissolved in 5 ml MeOH and stirred with light heating for 30 minutes. After this time, the precipitate that formed was filtered and washed with a further 2 ml MeOH and then re-dissolved in a small amount of MeCN. The solution so formed was placed in an open vessel within a vapour-diffusion chamber containing diethyl ether, yielding purple crystals that were suitable for X-ray crystallographic analysis. Mw 1163.43; Yield17 mg (60 %); IR (cm^{-1}, room temperature)3103 (s), 3074 (s), 2296 (s), 1609 (s), 1536 (s), 1495 (s), 1433 (s), 1399 (s), 1263 (s), 1248 (s), 1167 (s), 1079 (br), 882 (s), 846 (s), 793 (s), 756 (s), 732 (a), 671 (s), 653 (s), 619 (s); Anal. Found C 54.14, H 3.83, N 8.22; Calcd for C$_{50}$H$_{38}$N$_6$Fe$_3$Cl$_2$O$_8$, C 55.13, H 3.52, N 7.71.

Acknowledgements

Notes and references

^{a} *School of Chemistry, Building 23, Monash University, Clayton, Victoria, 3800, Australia. Fax: +613 99054597; Tel: +61399054512; E-mail: keith.murray@monash.edu*

1. (a) M. Clemente-León, E. Coronado and M. López-Jordà, *Eur. J. Inorg. Chem.*, 2013, 753; (b) O. Roubeau, M. Evangelisti and E. Natividad, *Chem. Commun.*, 2012, **48**, 7604; (c) S. Mossin, B. L. Tran, D. Adhikari, M. Pink, F. W. Heinemann, J. Sutter, R. K. Szilagyi, K. Meyer and D. J. Mindiola, *J. Am. Chem. Soc.*, 2012, **134**, 13651; (d) K. S. Murray, Chap. 1 in "*Spin-Crossover Materials; Properties and Applications*", ed. M. A. Halcrow, John Wiley and Sons, London, 2013, pp. 1 - 54.
2. T. Romero, R. A. Orenes, A. Espinosa, A. Tárraga and P. Molina, *Inorg. Chem.*, 2011, **50**, 8214.
3. (a) B. Balaji, B. Banik, P. K. Sasmal, B. Maity, R. Majumdar, R. R. Dighe and A. R. Chakravarty, *Eur. J. Inorg. Chem.,* 2012, 126; (b) B. Farlow, T. A. Nile, J. L. Walsh and T. A. McPhail, *J. Am. Chem. Soc.*, 1993, **12**, 2891.
4. H. S. Scott, A. Nafady, J. D. Cashion, A. M. Bond, B. Moubaraki, K. S. Murray and S. M. Neville, *Dalton Trans.,* 2013, **42**, 10326.
5. B. A. Leita, B. Moubaraki, K. S. Murray and J. P. Smith, *Polyhedron*, 2005, **24**, 2165.
6. C.-F. Sheu, K. Chen, S.-M. Chen, Y.-S. Wen, G.-H. Lee, J.-M. Chen, J.-F. Lee, B.-M. Cheng, H. S. Sheu, N. Yasuda, Y. Ozawa, K. Toriumi and Y. Wang, *Chem. Eur. J.*, 2009, **15**, 2384.
7. (a) T. Ayers, S. Scott, J. Goins, N. Caylor, D. Hathcock, S. J. Slattery and D. L. Jameson, *Inorg. Chim. Acta*, 2000, **307**, 7; (b) D. J. Hathcock, K. Stone, J. Madden and S. J. Slattery, *Inorg. Chim. Acta*, 1998, **282**, 131, and references therein.
8. (a) S. Hayami, Y. Komatsu, T. Shimizu, H. Kamihata and Y. H. Lee, *Coord. Chem. Rev*., 2011, **255**, 1982; (b) Y. H. Lee, M. S. Won, J. M. Harrowfield, S. Kawata, S. Hayami and Y. Kim, *Dalton Trans.,* 2013, **42**, 11507; (c) S. Hayami, R. Moriyama, Y. Shigeyoshi, R. Kawajiri, T. Mitani, M. Akita, K. Inoue and Y. Maeda, *Angew. Chem. Int. Ed*., 2005, **44**, 4899; (d) S. Hayami, M. R. Karim and Y. H. Lee, *Eur. J. Inorg. Chem*., 2013, 683.
9. (a) C. A. Kilner and M. A. Halcrow, *Dalton Trans*., 2010, **39**, 9008; (b) S. Kremer, W. Henke and D. Reinen, *Inorg. Chem*., 1982, **21**, 3013; (c) P. Nielsen, H. Toftlund, A. D. Bond, J. F. Boas, J. R. Pilbrow, G. R. Hanson, C. Noble, M. J. Riley, S. M. Neville, B. Moubaraki and K. S. Murray, *Inorg. Chem*., 2009, **48**, 7033.
10. (a) C. L. Raston and A. H. White, *J. Chem. Soc. Dalton Trans*., 1976, 7; (b) T. Takusagawa, P. G. Yohannes and K. B. Mertes, *Inorg. Chim. Acta*, 1968, **114**, 165; (c) H. Oshio, H. Spiering and P. Gütlich, *Inorg. Chem*., 2001, **40**, 1143.
11. V. Niel, A. B. Gaspar, M. C. Muñoz, B. Abarca, R. Ballesteros and J. A. Real, *Inorg. Chem*., 2003, **42**, 4782.
12. (a) J. E. Beves, E. C. Constable, C. E. Housecroft, C. J. Kepert, M. Neuburger, D. J. Price, S. Schaffner and J. A. Zampese, *Dalton Trans.*, 2008, 6742; (b) J. E. Beves, Ph.D. Thesis, "Crystal Engineering with 2,2':6',2"- Terpyridine Derivatives and their Metal Complexes: From simple building blocks to coordination polymers and networks", University of Basel; (c) J. E. Beves, D. J. Bray, J. K. Clegg, E. C. Constable, C. E. Housecroft, K. A. Jolliffe, C. J. Kepert, L. F. Lindoy, M. Neuburger, D. J. Price, S. Schaffner and F. Schaper, *Inorg. Chim. Acta*., 2008, **361**, 2582.
13. A. J. Bard and L. R. Faulkner, *Electrochemical Methods: Fundamentals and Applications*, 2Ed, John Wiley and Sons, London 1980

14. A. N. Simonov, P. Kemppinen, C. Pozo-Gonzalo, J. F. Boas, A. Bilic, A. D. Scully, A. Attia. A. Nafady, E. A. Mashkina, K. N. Winzenberg, S. E. Watkins and A. M. Bond, *J. Phys. Chem. B*, 2014, **118**, 6839

15. J. Zhang, A. M. Bond, W. J. Belcher, K. J. Wallace and J. W. Steed *J. Phys. Chem. B* **2003**, *107*, 5777

16. J. M. Rao, M. C. Hughes and D. J. Macero, *Inorg. Chim. Acta*, 1976, **16,** 232.

17. D. E. Morris, K. W. Hanck and K. DeArmond, *J. Electroanal. Chem.*, 1983, **149**, 115.

18. (a) P. M. Guha, H. Phan, J. S. Kinyon, W. S. Brotherton, K. Sreenath, J. T. Simmons, Z. Wang, R. J. Clark, N. S. Dalal, M. Shatruk and L. Zhu, *Inorg. Chem.*, 2012, **51**, 3465; (b) J. D. Crowley, P. H. Bandeen and L. R. Hanton, *Polyhedron*, 2010, **29**, 70; (c) M. Mydlak, C. Bizzarri, D. Hartmann, W. Sarfert, G. Schmid and L. De Cola, *Adv. Funct. Mater*, 2010, **20**, 1812; (d) M. Obata, A. Kitamura, A. Mori, C. Kameyama, J. A. Czaplewska, R. Tanaka, I. Kinoshita, T. Kusumoto, H. Hashimoto, M. Harada, Y. Mikata, T. Funabiki and S. Yano, *Dalton Trans.*, 2008, 3292.

19. C. M. Harris, T. N. Lockyer, R. L. Martin, H. R. H. Patil and E. Sinn, *Aust. J. Chem.*, 1969, **22**, 2105.

20. W. Kabsch, *J. Appl.Crystallogr.*, 1993, **26**, 795.

21. (a). G. M. Sheldrick, *SHELXL-97,Program for refinement of crystal structures*, University of Göttingen, Germany, 1997; (b). A. L. Spek, *Acta Crystallogr., Sect A: Fundam. Crystallogr.*, 1990, **46**, C34.

22. A. L. Spek, *J. Appl. Crystallogr.*, 2003, **36**, 7.

Ferrocene-appended ligands for use in spin crossover-redox "hybrid" complexes of iron(II) and cobalt(II)

Hayley S. Scott,[a] **Christopher J. Gartshore ,**[a] **Si-Xuan Guo,**[a] **Boujemaa Moubaraki,**[a] **Alan. M. Bond,**[a] **Stuart R. Batten,**[a] **and Keith S. Murray***[a]

GRAPHICAL ABSTRACT

The new complexes *trans*-$[Fe^{II}(FTP)_2(NCS)_2]$, $[Co^{II}(FTTP)_2](ClO_4)_2 \cdot 2(MeCN)$ and $[Fe^{II}(FTTP)_2](ClO_4)_2 \cdot Et_2O$ (where FTP = 4-(2-pyridyl)-1H-1,2,3-triazol-1-ylferrocene and FTTP = 4'-ferrocenyl-2,2':6',2''-terpyridine) display high spin d^6, spin crossover d^7 and low spin behaviour d^6, respectively, as judged by structural and magnetic studies. Electrochemical studies on solutions provide redox couples for the ferrocene moiety and central metals with unusual diffusion coefficients.
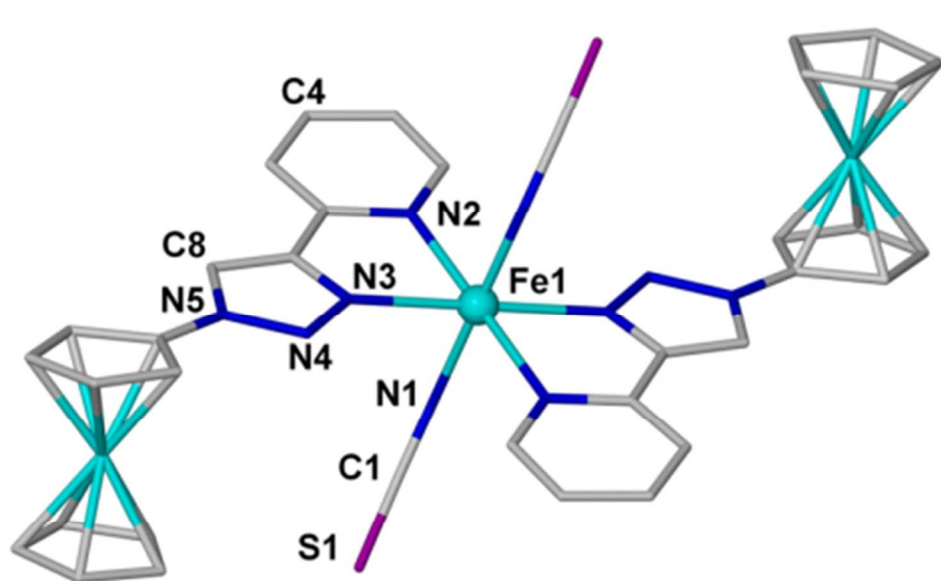
for graphical abstract
57x35mm (220 x 220 DPI)